Geophysical Journal International

Geophys. J. Int. (2018) **214,** 2236–2249
Advance Access publication 2018 June 20
GJI Geodynamics and tectonics

doi: 10.1093/gji/ggy245

A Boussinesq slurry model of the F-layer at the base of Earth's outer core

Jenny Wong,[1] Christopher J. Davies[2] and Chris A. Jones[3]

[1]*EPSRC Centre for Doctoral Training in Fluid Dynamics, University of Leeds, Leeds* LS2 9JT*, UK. E-mail: mm09j2w@leeds.ac.uk*
[2]*School of Earth and Environment, University of Leeds, Leeds* LS2 9JT*, UK*
[3]*Department of Applied Mathematics, University of Leeds, Leeds* LS2 9JT*, UK*

Accepted 2018 June 19. Received 2017 December 13; in original form 2018 April 16

SUMMARY

Seismic observations suggest that a stably stratified layer, known as the F-layer, 150–300 km thick exists at the bottom of Earth's liquid outer core. These observations contrast with the density inferred from the Preliminary Reference Earth Model (PREM), which assumes an outer core that is well-mixed and adiabatic throughout. The liquid core is composed primarily of iron alloyed with a light component. A thermal boundary layer produces the opposite effect on the density profile compared with the observations, and single phase, thermochemical models do not provide a sufficient dynamic description of how light element is transported across the F-layer into the overlying liquid outer core. We therefore propose that the layer can be explained by a slurry on the liquidus, whereby solid particles of iron crystallize from the liquid alloy throughout the layer. The slurry model provides a dynamic explanation of how light element can be transported across a stable layer. We make two key assumptions, the first of which is fast-melting where the timescale of freezing is considered short compared to other processes. The second assumption is that we consider a binary alloy where the light element is purely composed of oxygen, which is expelled entirely into the liquid during freezing. We present a steady state 1-D box model of a slurry formulated in a reference frame moving at the speed of inner core growth. We ascertain temperature, light element concentration and solid flux profiles by varying the layer thickness, inner core heat flux and thermal conductivity, since there is some uncertainty in these estimates. Our solutions demonstrate that the steady state slurry can satisfy the geophysical constraints on the density jump across the layer and the core–mantle boundary heat flux.

Key words: Composition and structure of the core; Core; Planetary interiors.

1 INTRODUCTION

It is well established that a seismically distinct layer is located at the base of the Earth's outer core (Souriau & Poupinet 1991; Zou *et al.* 2008; Adam & Romanowicz 2015; Ohtaki & Kaneshima 2015). This so-called 'F-layer' is characterized by an observed *P*-wave velocity, V_p, that is slower compared with the Preliminary Earth Reference Model (PREM) (Dziewonski & Anderson 1981). Souriau & Poupinet (1991) argued that density, ρ, rather than the bulk modulus, K, is more likely to vary in liquids at high pressure, and therefore inferred from the relationship $V_p^2 = K/\rho$ that the observed layer is denser than expected. PREM assumes that the liquid core is chemically homogeneous and adiabatically stratified throughout, so a slower V_p compared to PREM indicates stable stratification at the base of the outer core that cannot be explained by adiabatic compression alone.

The low V_p layer is consistently observed by seismology, however its thickness, d, is uncertain. Souriau & Poupinet (1991) and Song & Helmberger (1992) independently obtained $d \approx 150$ km. The AK135 (Kennett *et al.* 1995) reference model features a 400-km-thick layer. Zou *et al.* (2008) also observe a low V_p structure at the base of the outer core that is 350 km thick. More recently, a layer thickness of up to 380 km was reported by Ohtaki & Kaneshima (2015). On the other hand, Adam & Romanowicz (2015) prefer a 300-km-thick layer with a V_p gradient greater than that of AK135 on top of a 50-km-lower velocity layer directly above the inner core boundary (ICB). We consider here thicknesses in the range of $150 \leq d \leq 300$ km.

The existence of a stably-stratified layer at the base of the outer core has profound implications for understanding the geodynamo and core evolution. The principal energy sources for sustaining the present-day geodynamo are predominantly from compositional con-

vection due to the release of light element during inner core growth and thermal convection powered by secular cooling. Greater thermodynamic efficiency is achieved from compositional convection (Nimmo 2015) driven by light element passing through the F-layer into the overlying liquid outer core but it is presently unclear how this is achieved while preserving the stable stratification. Consequently, explaining the existence of the F-layer and how it may be sustained is of great geophysical interest.

The exact composition and abundance of light elements in the Earth's core are not precisely known, though geochemical arguments favour candidate elements such as oxygen, silicon and sulphur (e.g. Badro *et al.* 2015). Over time the core cools and the inner core solidifies and grows. First principles calculations have shown that for an Fe-(S,Si)-O mixture under core conditions, oxygen partitions entirely into the liquid upon solidification whereas silicon and sulphur partition evenly into the solid and liquid (Alfè *et al.* 2002b).

Previous work on the F-layer considers the possibility that a purely thermal boundary layer could exist at the base of the Earth's outer core. Slower fluid velocity close to the solid inner core inhibits convective mixing, therefore a super-adiabatic temperature is required to conduct heat out across the boundary layer. Density decreases with depth, since material at the bottom of the layer is hotter and more thermally buoyant than the material at the top. This set-up contradicts the seismically inferred density increase with depth, and therefore the F-layer cannot be explained by a thermal boundary layer (Gubbins *et al.* 2008).

Alternatively Gubbins *et al.* (2008) propose a two-component layer constrained to the liquidus temperature to explain the F-layer. The liquidus is the temperature that divides solid from liquid phase and it is dependent on pressure and light element concentration. Gubbins *et al.* (2008) assume a fixed layer thickness and impose a light element concentration at the boundaries to match a range of seismically determined density jumps, thus prescribing a compositionally stratified layer from the outset. The solutions are consistent with suggested CMB heat flows using a lower estimate of the thermal conductivity, however newly obtained thermal conductivity estimates are two to three times larger than previously thought (Pourovskii *et al.* 2017; Pozzo *et al.* 2014; Gomi *et al.* 2013) which will likely impact the results. The model outlined by Gubbins *et al.* (2008) does not explain the origin of compositional stratification since this is prescribed, and so a dynamic description how light material moves around and ultimately out of the layer is still needed.

Convective translation has been proposed as a possible mechanism for explaining the F-layer. This particular deformationless mode of motion can arise in convectively unstable conditions and results in inner core freezing in the Western Hemisphere and melting in the Eastern Hemisphere. Alboussière *et al.* (2010) use a low-thermal conductivity of 36 $\mathrm{W\,m^{-1}\,K^{-1}}$ that favours superadiabatic conditions for thermal convection, and a high critical viscosity on the order of 10^{18} Pa s accommodates convective instability by reducing viscous deformation. The viability of this mechanism may be limited by high-thermal conductivity estimates, which implies that the inner core is thermally stratified. Compositional effects have been proposed as an alternative pathway to inner core convection, since freshly created solid at the ICB over the lifetime of the inner core gives rise to unstable stratification as the concentration of iron is progressively refined (Deguen *et al.* 2013). Gubbins *et al.* (2013) find a weak chemical stratification caused by temperature dependent partitioning of light elements, though Labrosse (2014) and Lythgoe *et al.* (2015) find that unstable compositional effects are dominated by thermal stratification and so inner core convection is unlikely to occur. These models of convective translation are mainly concerned with explaining the hemispherical asymmetry of the inner core, and it is unclear whether the magnitude of this convection can explain an F-layer hundreds of kilometres thick.

This paper aims to establish the dynamics of a slurry that allows the passage of light material through the F-layer while retaining a stable stratification. We extend the two-component, single phase model by permitting a small amount of solid phase to crystallize and create a slurry layer. We envisage solid iron particles freezing throughout the slurry layer that sink under gravity towards the ICB to grow the inner core, whilst the remaining light material migrates to the outer core to power the dynamo without disturbing the stable stratification. Our model builds on the work of Loper & Roberts (1977, 1980, 1987) and Roberts & Loper (1987). Loper & Roberts (1977) developed a full general theory before reducing it by assuming that light element does not partition into the solid phase, and that the fast-melting limit applies. These two key approximations form the basis of our model.

A constant solid composition assumes that no light material is incorporated into the solid upon freezing. We assume that the core material can be approximated by a binary alloy composed of iron and oxygen, since oxygen is expelled entirely into the liquid when freezing an Fe-(S,Si)-O alloy, while silicon and sulphur are evenly partitioned between the liquid and solid (Alfè *et al.* 2002b). The constant solid assumption avoids the complex history dependence of particle size on processes such as diffusion and sedimentation of iron at previous locations with different conditions in pressure, temperature and composition. The fast-melting limit assumes that a change in phase occurs instantaneously compared with other relevant time-scales in the slurry. This simplifies the thermodynamics of the system so that regions of material can be clearly separated into slurry and slurry-free regions and constrains the slurry to the liquidus temperature, which is determined by the composition and pressure at every point in the layer. If the temperature at any point is higher than the liquidus temperature then the solid iron particles there would completely melt, while if the temperature is below the liquidus then the iron solidifies to release the latent heat necessary to raise the temperature to the liquidus. Fast-melting is an approximation used to good effect in other iron snow models such as Davies & Pommier (2018).

In this paper, we present a self-consistent, simplified model that elucidates the key features of a slurry, and find steady state solutions to compare with the geophysical observations. The slurry theory is developed in Section 2 along with the necessary boundary conditions for the steady state equations. Solutions to the model should satisfy the geophysical constraints, namely that the density jump across the layer should be consistent with seismology, and that the core–mantle boundary heat flux should be within plausible limits. Section 3 explores the effect of various layer thicknesses and ICB heat fluxes on the steady state, and investigates the effect of recent higher thermal conductivity estimates by comparing with a lower thermal conductivity (Konôpková *et al.* 2016). Section 4 summarises the results and discusses the main assumptions of the theory.

2 THEORY

The slurry model described in this section starts from the assumptions that the fast-melting limit applies and that the light element partitions entirely into the liquid upon solidification of the alloy (Loper & Roberts 1977). We consider a simple model of a binary slurry in a Cartesian box, with no magnetic field and no rotation.

A Boussinesq fluid is considered, where changes in density are assumed to be small except in the buoyancy force, since variations in core density are on the order of 0.1 per cent within hundreds of kilometres of the ICB according to PREM (Dziewonski & Anderson 1981). For reference a list of all parameters is given in Table (A1).

2.1 Basic definitions

The slurry consists of a two component mixture: light oxygen alloyed with heavy iron. Given that oxygen partitions entirely into the liquid upon solidification of the mixture (Alfè *et al.* 2002b), then oxygen is always in the liquid phase, whereas iron may either be in the solid or liquid phase. The components and phases are defined by considering a small volume of material with oxygen mass, M^l_{O}, liquid iron mass, M^l_{Fe}, and solid iron mass, M^s_{Fe}. Here the superscript denotes the phase, with l for liquid and s for solid, and the subscript denotes the composition, with O for oxygen and Fe for iron. The mass fractions of light element, ξ, light element in the liquid phase, ξ^l and solid, ϕ are defined as

$$\xi = \frac{M^l_{\mathrm{O}}}{M^l_{\mathrm{O}} + M^l_{\mathrm{Fe}} + M^s_{\mathrm{Fe}}} = \frac{\text{Light element mass}}{\text{Total mass}},$$

$$\xi^l = \frac{M^l_{\mathrm{O}}}{M^l_{\mathrm{O}} + M^l_{\mathrm{Fe}}} = \frac{\text{Light element mass}}{\text{Liquid mass}},$$

$$\phi = \frac{M^s_{\mathrm{Fe}}}{M^l_{\mathrm{O}} + M^l_{\mathrm{Fe}} + M^s_{\mathrm{Fe}}} = \frac{\text{Solid mass}}{\text{Total mass}}.$$

These definitions determine the relation

$$\xi = (1-\phi)\xi^l, \tag{1}$$

and its differential form

$$\mathrm{d}\xi = (1-\phi)\mathrm{d}\xi^l - \xi^l \mathrm{d}\phi, \tag{2}$$

which will be used to develop the slurry equations later.

2.2 Conservation equations

We assume that density variations are small relative to the reference density, so that the Boussinesq approximation can be used. The reference density is chosen to be the value for pure liquid iron, ρ^l_{Fe}, since the solid fraction in the slurry is small. Density variations are neglected everywhere except in the buoyancy term where they are multiplied by the gravitational acceleration. The total mass of a slurry is conserved, therefore

$$\nabla \cdot \mathbf{u} = \mathbf{0}, \tag{3}$$

where $\mathbf{u}$ is the slurry velocity. Conservation of light material in the slurry implies

$$\rho^l_{\mathrm{Fe}} \frac{\mathrm{D}\xi}{\mathrm{D}t} = -\nabla \cdot \mathbf{i}, \tag{4}$$

where $\mathbf{i}$ is the diffusive flux of light element (Landau & Lifshitz 1959; Loper & Roberts 1977). The solid fraction, ϕ, is not conserved as it can be created or destroyed through freezing or melting, hence

$$\rho^l_{\mathrm{Fe}} \frac{\mathrm{D}\phi}{\mathrm{D}t} = -\nabla \cdot \mathbf{j} + m^s, \tag{5}$$

where $\mathbf{j}$ is the solid flux of the iron particles and m^s is a source term that defines the rate solid particles are formed (Loper & Roberts 1977). Conservation of energy is given by

$$\rho^l_{\mathrm{Fe}} T \frac{\mathrm{D}s}{\mathrm{D}t} = -\nabla \cdot (T\mathbf{k}) - \mathbf{i} \cdot \nabla \mu^l, \tag{6}$$

where T is the temperature, s is the entropy, $\mu^l = \mu^l_{\mathrm{Fe}} - \mu^l_{\mathrm{O}}$ is the chemical potential of the mixture in the liquid phase, which is the free energy released when an atom of liquid oxygen replaces an atom of liquid iron at constant p and T, and $\mathbf{k}$ is the entropy flux vector (see eq. 5.26, Loper & Roberts 1977). The viscous dissipation is zero because of the Boussinesq approximation, while internal heating and the heat of reaction are ignored. Constitutive relations for the light element flux, $\mathbf{i}$, solid flux, $\mathbf{j}$, and entropy flux, $\mathbf{k}$, are derived in Section2.3, eqs (18)–(21).

The momentum equation under the Boussinesq approximation, with no rotation and no magnetic field, is given by

$$\frac{\mathrm{D}\mathbf{u}}{\mathrm{D}t} = -\nabla\left(\frac{p'}{\rho^l_{\mathrm{Fe}}}\right) - \frac{\rho'}{\rho^l_{\mathrm{Fe}}} g\hat{\mathbf{z}} + \nu\nabla^2\mathbf{u} + \mathbf{F}, \tag{7}$$

where p' is the non-hydrostatic pressure, ρ' is the density variation due to buoyancy, g is gravitational acceleration, $\hat{\mathbf{z}}$ is the vertical unit vector of the Cartesian box, pointing outwards and away from the ICB, ν is the kinematic viscosity and $\mathbf{F}$ are other general body forces. The density variation, ρ', is given by

$$\rho' = \rho^l_{\mathrm{Fe}}\left[-\alpha T' - \alpha_\xi \xi' + \alpha_\phi \phi'\right], \tag{8}$$

where α is the thermal expansion coefficient, α_ξ is the compositional expansion coefficient, $\alpha_\phi = -\rho^l_{\mathrm{Fe}}(\partial V/\partial\phi)_{T,\xi}$ is the phasal expansion coefficient, and the primes denote the perturbations from the reference value [see eqs (A2) and (A3)].

2.3 The liquidus and constitutive relations

The differential of the Gibbs free energy, without assuming a constant solid composition for the moment, is (Loper & Roberts 1977)

$$\begin{aligned}\mathrm{d}\Phi = {} & V\mathrm{d}p - s\mathrm{d}T + \mu^l \mathrm{d}\xi + \phi\left(\mu^s - \mu^l\right)\mathrm{d}\xi^s \\ & + \left[\mu_\phi - (\xi^s - \xi^l)\mu^l\right]\mathrm{d}\phi,\end{aligned} \tag{9}$$

where ξ^s is light element in the solid phase, V is the specific volume, $\mu^s = \mu^s_{\mathrm{Fe}} - \mu^s_{\mathrm{O}}$ is the chemical potential of iron relative to light element in the solid phase, which is the free energy released when an atom of solid oxygen replaces an atom of solid iron at constant p and T, and $\mu_\phi = \left(\frac{\mathrm{d}\Phi}{\mathrm{d}\phi}\right)_{p,T,\xi^l,\xi^s} = \Phi^s - \Phi^l$ is the chemical potential of solid relative to the liquid phase, which is also the difference between the solid and liquid part of the Gibbs free energy (see the Lever rule in Appendix A). Phase change ($\mathrm{d}\phi \neq 0$) at constant pressure, temperature and ξ requires $\mathrm{d}\Phi = 0$ to minimize the Gibbs free energy at equilibrium, therefore

$$\mu_\phi - (\xi^s - \xi^l)\mu^l = 0. \tag{10}$$

If we briefly consider a variation in solid light element ($\mathrm{d}\phi = 0$ and $\mathrm{d}\xi^s \neq 0$), then $\mu^l = \mu^s$. The constant solid assumption, in which $\xi^s = 0$, means that μ^s no longer enters the theory as phase equilibrium implies $\mu^l = \mu^s$ everywhere, so μ^l is rewritten as μ with no danger of ambiguity henceforth. Assuming that the liquid and solid phases do not interact chemically, which is commonly supposed in phase equilibrium, then the Lever rule can apply where the Gibbs free energy is assumed linear in ϕ. Hence the phase equilibrium condition (10) is equivalent to

$$\Phi^s - \Phi^l + \xi^l \mu = 0, \tag{11}$$

where Φ^s denotes Gibbs free energy of the solid and Φ^l denotes the Gibbs free energy of the liquid. The differential of (11) is also equal

to zero at phase equilibrium, so

$$\begin{aligned} \mathrm{d}\Phi^s &= V^s \mathrm{d}p - s^s \mathrm{d}T, \\ \mathrm{d}\Phi^l &= V^l \mathrm{d}p - s^l \mathrm{d}T + \mu \mathrm{d}\xi^l, \\ \mathrm{d}\mu &= \Delta V^l_{\mathrm{Fe,O}} \mathrm{d}p + \frac{\partial \mu}{\partial T}\mathrm{d}T + \frac{\partial \mu}{\partial \xi^l}\mathrm{d}\xi^l, \end{aligned} \tag{12}$$

yields the liquidus relation

$$\Delta V^{s,l}_{\mathrm{Fe}} \mathrm{d}p - \frac{L}{T}\mathrm{d}T = \xi^l \frac{\partial \mu}{\partial \xi^l}\mathrm{d}\xi^l, \tag{13}$$

where

$$\begin{aligned} -\Delta V^{s,l}_{\mathrm{Fe}} &= -\Delta V^{s,l}_{\mathrm{Fe,O}} + \xi^l \Delta V^l_{\mathrm{Fe,O}}, \\ \frac{L}{T} &= -s^s + s^l + \xi^l \frac{\partial \mu}{\partial T}. \end{aligned}$$

Full details are included in Appendix A.

To complete the conservation equations, the constitutive form of the light material flux **i**, solid flux **j** and entropy flux **k** must be sought. We invoke the Onsager reciprocal relations together with the fast-melting limit to obtain

$$\mathbf{i} = -a\nabla\mu - g\nabla T - \xi^l \mathbf{j} \tag{14}$$

$$\mathbf{j} = b\xi^l \nabla\mu - f\nabla T \tag{15}$$

$$\mathbf{k} = -(g - f\xi^l)\nabla\mu - c\nabla T. \tag{16}$$

where a, b, c, f and g are coefficients to be determined (see eqs 2.1 and 2.2 of Loper & Roberts 1980). Small-scale responses of the light element mass flux to temperature gradients, also known as the Soret effect, are usually ignored (Gubbins *et al.* 2004), and the solid flux is independent of temperature and compositional gradients, therefore we must have (Loper & Roberts 1980)

$$\begin{aligned} f &= -b\left(\frac{L}{T} - \xi^l \frac{\partial \mu}{\partial T}\right), \\ g &= -a\frac{\partial \mu}{\partial T}. \end{aligned} \tag{17}$$

Upon substitution of (12), (13) and (17) into (14), the light element flux becomes

$$\mathbf{i} = -\frac{\rho^l_{Fe} D' \Delta V^{s,l}_{Fe,O}}{\xi^l \left(\partial\mu/\partial\xi^l\right)}\nabla p + \frac{\rho^l_{Fe} D' L}{T\xi^l \left(\partial\mu/\partial\xi^l\right)}\nabla T - \xi^l \mathbf{j}, \tag{18}$$

where $a \equiv \rho^l_{\mathrm{Fe}} D' / \left(\partial\mu/\partial\xi^l\right)$ (Landau & Lifshitz 1959), and D' is the self-diffusion coefficient of the light material. The first term in (18) corresponds to the barodiffusion of light material in the slurry and occurs whether solid material is present or not. Variations in $\nabla\xi^l$ depend on ∇p and ∇T through the liquidus, which is the cause of the 'Soret'-like behaviour in the second term of (18). The last term accounts for the light element that is displaced by the flux of solid particles snowing towards the ICB under gravity.

Substituting (12) and (17) into (15) and eliminating $\nabla\xi^l$ via the liquidus (13) yields the solid flux

$$\mathbf{j} = b(\phi)\Delta V^{s,l}_{Fe,O}\nabla p, \tag{19}$$

where $b(\phi)$ is the sedimentation coefficient. The mass flux, **j**, describes how the solid particles fall through the liquid in response to a pressure gradient. The sole purpose of the sedimentation coefficient is to relate the solid fraction, ϕ, with the solid flux, **j**. This can potentially be described by a variety of elaborate crystal growth models. For the sake of simplicity, we assume the iron snow flakes are spherical particles falling with gravity against viscous drag, known as Stokes flow. This gives

$$b(\phi) \equiv k_\phi \phi^{5/3} = \left[\frac{\rho^s_{\mathrm{Fe}}(\rho^l_{Fe})^2}{162\pi^2\nu^3 N^2}\right]^{1/3} \phi^{5/3}, \tag{20}$$

where N is the number of particles per unit volume. This model of mobility is valid in the limit of $\phi \ll 1$. If ϕ exceeds a critical value, then the slurry transitions to a solid matrix of mush, an effect that is not supported by the current theory. If there are a small number of very large particles or a large number of very small particles, then both scenarios can produce the same solid flux. There is no likely indication of what the particle size should be from observations to constrain N, hence by considering solutions of **j** there is no need to evaluate $b(\phi)$. Other more sophisticated models of crystal growth and mobility [for example, crystallization of magma oceans (Solomatov 2007)] could be incorporated into $b(\phi)$ to account for factors such as particle shapes and hindered particle transport.

The entropy flux can be written (Loper & Roberts 1980)

$$\mathbf{k} = -\frac{\partial \mu}{\partial T}\mathbf{i} - \frac{L}{T}\mathbf{j} - \frac{k}{T}\nabla T. \tag{21}$$

Together with the entropy differential, ds, derived using the Gibbs free energy and Lever rule (see Appendix A), the energy equation (6) becomes

$$\rho^l_{\mathrm{Fe}} c_p \frac{\mathrm{D}T}{\mathrm{D}t} = \nabla\cdot(k\nabla T + L\mathbf{j}) + \rho^l_{\mathrm{Fe}} L \frac{\mathrm{D}\phi}{\mathrm{D}t}, \tag{22}$$

where $\mathrm{d}\xi^l$ has been eliminated in favour of dp and dT via the liquidus, and the heat of reaction and pressure freezing are neglected (Gubbins *et al.* 2003).

2.4 Governing equations and parameter estimates

In summary, the general equations of a Boussinesq slurry are

$$\xi = (1-\phi)\xi^l \tag{23a}$$

$$\rho^l_{\mathrm{Fe}} \frac{\mathrm{D}\xi}{\mathrm{D}t} = -\nabla\cdot\mathbf{i} \tag{23b}$$

$$\rho^l_{\mathrm{Fe}} \frac{\mathrm{D}\phi}{\mathrm{D}t} = -\nabla\cdot\mathbf{j} + m^s \tag{23c}$$

$$\rho^l_{\mathrm{Fe}} c_p \frac{\mathrm{D}T}{\mathrm{D}t} = \nabla\cdot(k\nabla T + L\mathbf{j}) + \rho^l_{\mathrm{Fe}} L \frac{\mathrm{D}\phi}{\mathrm{D}t} \tag{23d}$$

$$\frac{\mathrm{d}T}{\mathrm{d}z} = \frac{T\Delta V^{s,l}_{\mathrm{Fe}}}{L}\frac{\mathrm{d}p}{\mathrm{d}z} - \frac{T\xi^l\left(\partial\mu/\partial\xi^l\right)}{L}\frac{\mathrm{d}\xi^l}{\mathrm{d}z} \tag{23e}$$

$$\mathbf{i} = -\frac{\rho^l_{\mathrm{Fe}} D' \Delta V^{s,l}_{\mathrm{Fe,O}}}{\xi^l\left(\partial\mu/\partial\xi^l\right)}\nabla p + \frac{\rho^l_{\mathrm{Fe}} D' L}{T\xi^l\left(\partial\mu/\partial\xi^l\right)}\nabla T - \xi^l\mathbf{j} \tag{23f}$$

$$\mathbf{j} = b(\phi)\Delta V^{s,l}_{\mathrm{Fe,O}}\nabla p \tag{23g}$$

$$\nabla\cdot\mathbf{u} = 0 \tag{23h}$$

$$\frac{\mathrm{D}\mathbf{u}}{\mathrm{D}t} = -\nabla\left(\frac{p'}{\rho^l_{\mathrm{Fe}}}\right) - \frac{\rho'}{\rho^l_{\mathrm{Fe}}} g\hat{\mathbf{z}} + \nu\nabla^2\mathbf{u} + \mathbf{F} \tag{23i}$$

$$\rho' = \rho^l_{\mathrm{Fe}}\left[-\alpha T' - \alpha_\xi \xi' + \alpha_\phi \phi'\right]. \tag{23j}$$

The above equations may be solved iteratively. Relation (23a) together with the liquidus (23e) reduces the five thermodynamic

variables $\{p, T, \xi, \xi^l, \phi\}$ to three. Solving the energy equation (23d) yields the temperature, T, which then determines ξ^l from the liquidus (23e). The light element equation, (23b), determines ξ, which also determines ϕ through relation (23a). Eq. (23c) determines the freezing rate, m^s, which feeds back into the energy equation in the next iteration.

Slurry behaviour is fundamentally distinct from thermochemical convection. For example, in a system at constant pressure hot fluid does not necessarily rise as it does in regular thermal convection, since an increase in temperature reduces the concentration of light material in the liquid phase to maintain the liquidus. The increase in density from the reduction of light material can outweigh the decrease in density from the increasing temperature, therefore producing a stabilizing, bottom heavy layer. The most interesting feature of this model is encapsulated in light element equation (23b), as it describes how light element can pass through a stably-stratified layer. Light element can diffuse along a pressure gradient (barodiffusion) or temperature gradient ('Soret'-like effect), or be displaced upwards through the layer as solid particles sediment and fall towards the ICB under gravity.

Given that the F-layer is thin compared to the rest of the outer core, some parameter values are taken as constant since they do not vary much across the layer, such as the specific heat capacity, c_p, latent heat, L, thermal, α, compositional, α_ξ, and phasal, α_ϕ, expansion coefficients and isothermal compressibility, β. Values used are listed in Table A1.

Ideal solution theory is used to estimate the specific volumes V^l_{Fe}, V^s_{Fe} and V^l_{O}, of the slurry mixture. An ideal solution experiences no change in volume upon mixing. The validity of an ideal solution under core pressure and temperature conditions remains to be checked by high pressure experiments or theoretical calculations. Gubbins *et al.* (2004) argue that the ideal solution approximation should be accurate for small concentrations of impurity, and the specific densities are given by $\rho_{\mathrm{O}} = 5.56 \times 10^2\,\mathrm{kg\,m^{-3}}$, $\rho^s_{\mathrm{Fe}} = 12.76 \times 10^3\,\mathrm{kg\,m^{-3}}$ and $\rho^l_{\mathrm{Fe}} \equiv \rho^s_{\mathrm{Fe}} - \Delta\rho_{\mathrm{melting}} = 12.52 \times 10^3\,\mathrm{kg\,m^{-3}}$, where the density drop upon melting is $\Delta\rho_{\mathrm{melting}} = 0.24 \times 10^3\,\mathrm{kg\,m^{-3}}$ (Alfè *et al.* 2002a). This assumes that the core material is composed of an Fe-(Si,S)-O alloy, with 84 per cent iron, 8 per cent silicon/sulphur and 8 per cent oxygen, where oxygen partitions entirely into the liquid when the alloy solidifies (Alfè *et al.* 2002b).

The depression of the liquidus (23e) due to composition, and thus the light element flux (23f), depends on the derivative of the chemical potential with respect to ξ^l. We use ideal solution theory (Gubbins *et al.* 2004) to approximate the chemical potential by

$$\mu = \mu_0 + RT\frac{1000}{a_{\mathrm{O}}}\ln\xi^l,$$

where μ_0 is a constant and $R \times 1000/a_{\mathrm{O}}$ converts from molar to mass concentration, with R the gas constant and a_{O} the atomic weight of oxygen. Its thermodynamic derivative with respect to ξ^l is therefore

$$\xi^l\frac{\partial\mu}{\partial\xi^l} = RT\frac{1000}{a_{\mathrm{O}}}. \tag{24}$$

Since ξ^l cannot diffuse through solid material, Loper & Roberts (1980) suggest that the diffusion coefficient D' can be linearly approximated as

$$D' = (1-\phi)\bar{D}, \tag{25}$$

where $\bar{D}$ is now a modified diffusion coefficient independent of ϕ. First principles molecular dynamic simulations obtain $\bar{D} \approx 10^{-8}\,\mathrm{m^2 s^{-1}}$ (Pozzo *et al.* 2013).

Thermal conductivity at core conditions is difficult to calculate, and its value significantly impacts thermal history models. Lower thermal conductivity estimates found a nominal inner core age of a billion years (Labrosse *et al.* 2001). However, recent higher conductivity estimates mean that the inner core is a much younger feature of the Earth with an approximate age of 500 Myr (Nimmo 2015; Gomi *et al.* 2013; Davies *et al.* 2015).

2.5 Steady state

The slurry layer is considered to be relatively thin compared to the rest of the core, so we seek a reference state in a Cartesian geometry, with $\hat{\mathbf{z}}$ the unit vector pointing away from the ICB. With the aim of formulating a 1-D model, we assume no x, y dependence $(\frac{\partial}{\partial x}, \frac{\partial}{\partial y} \to 0)$. The position of the ICB advances upwards at the rate of inner core growth as solid particles accumulate at the base of the layer. In a steady state, the slurry is time-independent $\left(\frac{\partial}{\partial t} \to 0\right)$ and static $(\mathbf{u} = \mathbf{0})$. The time dependence of the advancing ICB is removed by transforming to a frame of reference that moves with the ICB, in a similar manner to Gubbins *et al.* (2008). This transformation is given by

$$z = z' - vt \qquad t = t', \tag{26}$$

where z' and t' are the vertical and time coordinates in the rest frame, with z and t the corresponding coordinates in the moving frame in which the ICB advances at a constant speed $v > 0$. In the moving frame in a steady state, the material derivative is given by

$$\frac{\mathrm{D}f}{\mathrm{D}t} \equiv -v\frac{\mathrm{d}f}{\mathrm{d}z}, \tag{27}$$

for an arbitrary scalar function, f. The light element (23b) and temperature (23d) equations for a slurry system with an advancing ICB become

$$\xi^l\frac{\mathrm{d}j_z}{\mathrm{d}z} = g\rho^l_{\mathrm{Fe}}\frac{\mathrm{d}}{\mathrm{d}z}\left(\frac{\rho^l_{\mathrm{Fe}}\bar{D}\Delta V^{s,l}_{\mathrm{Fe,O}}}{RT\frac{1000}{a_O}}\right) - \left(v\rho^l_{\mathrm{Fe}} + j_z\right)\frac{\mathrm{d}\xi^l}{\mathrm{d}z}, \tag{28}$$

$$-k\frac{\mathrm{d}^2T}{\mathrm{d}z^2} = v\rho^l_{Fe}c_p\frac{\mathrm{d}T}{\mathrm{d}z} + L\frac{\mathrm{d}j_z}{\mathrm{d}z}, \tag{29}$$

where the liquidus (23e) closes the equations, and the z-component of the solid flux, j_z, is given by (23g). Terms involving $\mathrm{d}\phi/\mathrm{d}z$ are ignored since the solid fraction is small and not expected to vary much in the layer.

2.6 Boundary conditions

The steady state equations (28), (29) and liquidus (23e) must be solved subject to four boundary conditions. We assume that the layer thickness, d, is fixed and cannot grow or shrink over time. Continuity of ξ^l at the core slurry boundary (CSB) at the top of the layer yields the condition $\xi^l(d) = \xi_T$, where ξ_T is the outer core concentration of light element and is presumed to be 8 mol. per cent of oxygen (Alfè *et al.* 2002b).

The total energy of the system is conserved, therefore

$$\mathbf{n}\cdot\langle\mathbf{k}\nabla\mathbf{T}\rangle = \mathbf{0} \tag{30}$$

after ignoring Soret effects, viscous stress and the heat of reaction (see eq. 3.23, Loper & Roberts 1987). Note that $\langle a\rangle = a^{sl} - a^{l/s}$ is the jump in an arbitrary quantity a, with superscripts sl and l/s denoting the value in the slurry and in the liquid/solid respectively.

At the ICB this becomes

$$\frac{\mathrm{d}T^{sl}}{\mathrm{d}z} = -\frac{Q_s^i}{k}, \tag{31}$$

where Q_s^i is the secular cooling of the inner core. Note that the latent heat flux is not included in this boundary condition, since we assume that the growth of the inner core is entirely due to the accumulation of solid particles from the slurry settling onto the ICB. This also means that no new particles nucleate at the boundaries and so solid is conserved, therefore applying the standard pill-box argument (Loper & Roberts 1987) to (23c) gives

$$\mathbf{n}\cdot\langle\rho\phi\,(\mathbf{u}-\mathbf{U})\rangle + \mathbf{n}\cdot\langle\mathbf{j}\rangle = \mathbf{0}, \tag{32}$$

where $\mathbf{U}$ is the boundary velocity. At the ICB, condition (32) becomes

$$\begin{aligned}\rho^{sl}\phi^{sl}(u^{sl}-U^{sl}) + j_z^{sl} - \rho^s\phi^s(u^s-U^s) - j_z^s = 0\\ \Rightarrow\ j_z^{sl} = -\rho_{Fe}^s v\end{aligned} \tag{33}$$

where $U^{sl} = U^s = v$, the velocity of the ICB and $\phi^{sl} \ll 1$ in the slurry. Here we use the fact that $\rho^{sl} \approx \rho^s$, $u^s = u^{sl} = j_z^s = 0$, and $\phi^s = 1$ in the solid inner core. The sign of the solid flux is negative down towards the ICB since iron particles sediment under gravity. Growth speed, v, is estimated by

$$v = \frac{r_i}{\tau_i} \tag{34}$$

where r_i is the present-day inner core radius and τ_i is the age of the inner core. Speeds of 1.2 and 2.4 mm yr^{-1} correspond with inner core ages of 0.5 and 1 Ga, respectively, and relate to the high and low values of thermal conductivity through the core energy budget (Davies *et al.* 2015). At the CSB condition (32) gives

$$\begin{aligned}\rho^{sl}\phi^{sl}(u^{sl}-U^{sl}) + j_z^{sl} - \rho^l\phi^l(u^l-U^l) - j_z^l = 0\\ \Rightarrow\ j_z^{sl} = 0,\end{aligned} \tag{35}$$

where $j_z^l = \phi^l = 0$ in the liquid since no solid exists on the liquid side of the CSB. Applying two boundary conditions on j_z over-constrains the steady state problem, therefore a free parameter is introduced as follows to ensure (35) is satisfied, so that the solid flux vanishes at the CSB.

We envisage a thin turbulent mixing sublayer at the top of the slurry generated by the difference in the slurry and the liquid outer core velocities. In the mixing sublayer diffusion is enhanced by eddies that promote the transport of light element out of the slurry layer into the rest of the outer core. This mechanism is incorporated into the pre-existing light element barodiffusion term in (28), as this process also transports light element out of the layer, albeit along a pressure gradient. Enhancement is controlled by modifying the self-diffusion coefficient, $\bar{D}$. A functional form of $\bar{D}$ is assumed by the exponential function

$$\bar{D} = D_0 \exp\left(\frac{Fz}{d}\right), \tag{36}$$

where $D_0 \approx 10^{-8}$ m^{2}s^{-1} and F is a dimensionless free parameter to be determined by forcing the solid flux to vanish at the CSB as required by (35). Note that the product rule now applies to the z-derivative of the barodiffusion term in (28).

2.7 Geophysical constraints

The steady-state model should satisfy several geophysical constraints. The density jump across the slurry layer should be consistent with seismic observations. Gubbins *et al.* (2008) noted that estimates of the density jump from normal mode studies, $\Delta\rho_{\mathrm{mod}}$, which have a resolution of several hundred kilometres, were generally larger than estimates from body waves, $\Delta\rho_{\mathrm{bod}}$, which have a high resolution of only a few kilometres. They suggested that $\Delta\rho_{\mathrm{bod}}$ represented the actual density jump across the ICB itself, but that $\Delta\rho_{\mathrm{mod}}$ included the density jump across the stable layer as well because of the lower resolution. The difference, $\Delta\rho_{\mathrm{mod}} - \Delta\rho_{\mathrm{bod}}$, therefore represents the density jump across the stable layer. There is considerable variation in the published estimates of $\Delta\rho_{\mathrm{mod}}$ and $\Delta\rho_{\mathrm{bod}}$. PREM gives $\Delta\rho_{\mathrm{mod}} = 600$ kg m^{-3} (Dziewonski & Anderson 1981) and other values can range up to $\Delta\rho_{\mathrm{mod}} = 820 \pm 180$ kg m^{-3} (Masters & Gubbins 2003). Body wave observations are as low as $\Delta\rho_{\mathrm{bod}} = 520 \pm 240$ kg m^{-3} (Koper & Dombrovskya 2005; Koper & Pyle 2004), and as high as $\Delta\rho_{\mathrm{bod}} = 1100$ kg m^{-3} (Tkalčić *et al.* 2009). The high $\Delta\rho_{\mathrm{bod}}$ estimate indicates that there is no detectable density jump across the stable layer. The highest $\Delta\rho_{\mathrm{mod}}$ data (Masters & Gubbins 2003) is $820 + 180 = 1000$ kg m^{-3}, and the lowest $\Delta\rho_{\mathrm{bod}}$ data (Koper & Dombrovskya 2005; Koper & Pyle 2004) is $520 - 240 = 280$ kg m^{-3}, giving a maximum possible stable layer density jump of $1000 - 280 = 720$ kg m^{-3}, which constrains the maximum density jump in our slurry model to be consistent with the seismic results. The variance in the range of permissible density jumps is attributed to the limitations of different sampling techniques employed in each seismic study (Deuss 2014).

Total density is given by the addition of the hydrostatic part together with density fluctuations (23j) within the slurry. The hydrostatic contribution is

$$\rho_H = \left(\beta g(z-d) + \frac{1}{\rho(d)}\right)^{-1}, \tag{37}$$

with $\rho(d)$ coincident with the PREM value at the top of the layer. Note that for a bottom-heavy layer the calculated density jump, $\Delta\rho$, is negative, so its magnitude is presented in the results.

The heat flux across the CMB should be within acceptable limits consistent with the core thermal history. Secular cooling of the core volume, Q_s, latent heat release from inner core growth, Q_l, and the gravitational energy, Q_g, contribute to the CMB heat flux. The gravitational energy is neglected in the slurry because of the Boussinesq approximation since there is no viscous or ohmic dissipation to balance the buoyancy flux in the F-layer (Anufriev *et al.* 2005), but is retained in the rest of the core as in Gubbins *et al.* (2004). Pressure freezing is ignored since it is believed to be small (Gubbins *et al.* 2004), and radiogenic heating is ignored for simplicity. Present day estimates of the maximum CMB heat flow are believed to be 12 ± 5 TW (Lay *et al.* 2008), and a minimum of 5 TW is deemed insufficient to power the geodynamo (Davies *et al.* 2015). Therefore acceptable steady state solutions should satisfy

$$5\ \mathrm{TW} \le Q^c = Q_s + Q_l + Q_g \le 17\ \mathrm{TW}, \tag{38}$$

where the secular cooling term, Q_s, is separated into three parts: the secular cooling of the inner core, Q_s^i, the slurry layer Q_s^{sl} and the rest of the adiabatic liquid outer core, $Q_s^{o'}$. In general, the secular cooling is given by

$$Q_s = -\int_V \rho c_p \frac{\mathrm{D}T}{\mathrm{D}t}\mathrm{d}V, \tag{39}$$

where $\mathrm{D}T/\mathrm{D}t = -v\mathrm{d}T_a/\mathrm{d}z$ in the inner core and outer core [assuming the inner core is adiabatically stratified (Labrosse *et al.* 2001)], $\mathrm{D}T/\mathrm{D}t = -v\mathrm{d}T_l/\mathrm{d}z$ using the liquidus gradient in the slurry and V is the relevant volume of the inner core, slurry or the rest of the outer core. The total ICB heat flux at the lower boundary, $Q^i = Q_s^i + Q_l$,

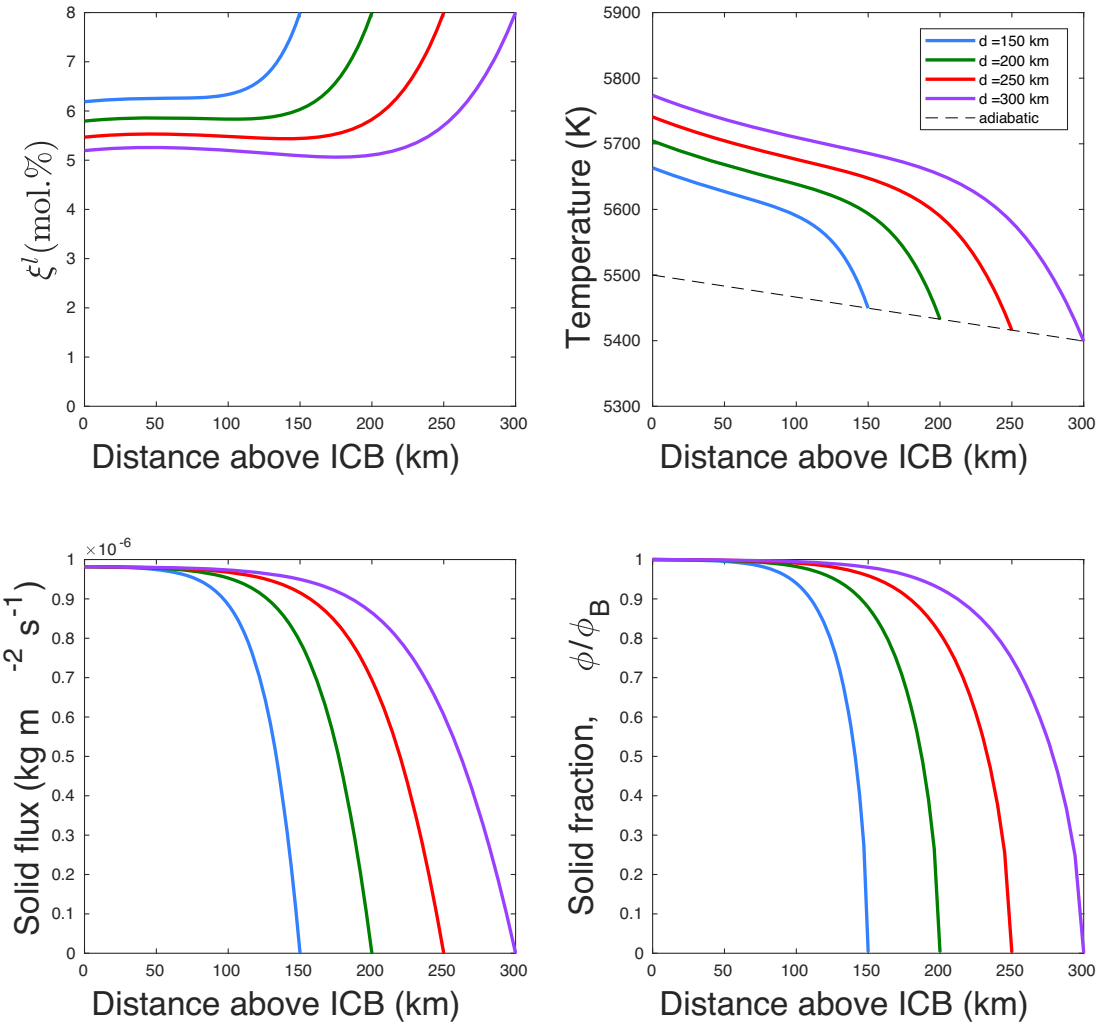

Figure 1 (Clockwise from top left) Profiles of ξ^l, temperature, solid fraction normalized by its value at the base of the layer, ϕ_B, and the solid flux. Layer thickness is indicated by the legend (colour online). Secular cooling of the inner core is fixed at $Q_s^i = 1.6$ TW and the thermal conductivity is equal to 107 W m^{-1} K^{-1}, with an inner core age of $\tau_i = 0.5$ Ga.

contains the latent heat flux,

$$Q_l = \int_{A^i} L j_z \, \mathrm{d}A^i, \tag{40}$$

where A^i is the surface area of the inner core. The latent heat flux, Q_l, is not known *a priori* since no freezing occurs directly at the ICB, and only the controlling parameter, the secular cooling of the inner core, Q_s^i, is input into the boundary condition (31). Gravitational power over the rest of the outer core, excluding the F-layer, is given by

$$Q_g = \int_V \rho \psi \alpha_\xi \frac{\mathrm{D}\xi}{\mathrm{D}t} \mathrm{d}V_{o'}, \tag{41}$$

where ψ is the gravitational potential and $\mathrm{D}\xi/\mathrm{D}t = -v\mathrm{d}\xi/\mathrm{d}z$. In conventional thermal history models the CMB heat flux is directly proportional to the core cooling rate $\mathrm{d}T_c/\mathrm{d}t$ (Nimmo 2015). When a slurry is present this is not the case, because the secular cooling in the slurry layer is conducted along the liquidus temperature gradient rather than the adiabat. As a result, the slurry solutions are characterized in terms of the inner core secular cooling.

3 RESULTS

We investigate the effect of layer thickness, variations of the ICB heat flux and the impact of high versus low thermal conductivity on a non-convecting, steady state slurry layer. All of the solutions should be consistent with geophysical constraints such as the seismic density jump across the layer, and give plausible CMB heat fluxes. All other parameters are kept fixed as listed in Table A1.

3.1 Effect of layer thickness and ICB heat flux

Given the range of layer depths inferred from seismology in Section 1 and the uncertainty in estimates of the ICB heat flux, layer thicknesses between 150 and 300 km at different rates of inner core secular cooling, Q_s^i, are investigated. Initially a fixed thermal conductivity of 107 W m^{-1} K^{-1} (Davies *et al.* 2015) with a young inner core age of 0.5 Ga is investigated.

Figure 1 shows profiles of ξ^l, T, j_z and ϕ/ϕ_B (the solid fraction normalized by its value at the base of the layer, ϕ_B) for a range of depths with $Q_s^i = 1.6$ TW. An increase in light element concentration to the outer core value of 8 mol. per cent is clearly observed, and its depressing effect on the liquidus towards the top of the layer

is evidenced by the steepening temperature gradient. Throughout the layer the solid flux remains close to its value predetermined by the inner core growth rate at the ICB and then quickly decreases to zero at the top, where the effect of barodiffusion is enhanced by the turbulent mixing layer. The solid fraction profile follows the behaviour of the solid flux governed through using Stokes flow as a model of mobility (20). The temperature at the CSB is continuous, hence at the top of the layer the liquidus temperature is equal to the adiabatic temperature, which is anchored at the ICB by the melting temperature, $T_i = 5500$ K (Nimmo 2015). A departure in temperature from this anchor point is evident at the base of the layer, since the actual temperature at the ICB increases due to the latent heat transported there by falling solid particles that have crystallized in the slurry. The slurry has developed an equilibrium by balancing the latent heat released by the freezing snow with the heat lost by cooling so that the temperature is on the liquidus everywhere in the layer.

3.2 Effect of thermal conductivity and inner core age

We compare lower estimates of the thermal conductivity to the solutions obtained with a higher thermal conductivity. A lower value of $k = 50\,\mathrm{W\,m^{-1}\,K^{-1}}$ (Konôpková *et al.* 2016), and an older inner core age of 1 Ga is selected. The steady state is sensitive to the inner core age through the speed of ICB advance, v, defined at the base of the slurry, and this enters the boundary condition (33) for the solid flux.

Profiles for a range of depths with a fixed secular cooling of $Q_s^i = 0.8$ TW are given in Figure 2. The speed of ICB advance has halved, resulting in the same factor of reduction in the solid flux imposed at the base of the layer. In comparison to the higher thermal conductivity solutions the reduction in solid flux yields a reduction in the light element concentration at the ICB, as less freezing occurs to partition light element into the liquid. Less light element in the liquid overall reduces the depression in the liquidus temperature. A lower thermal conductivity restricts the amount of heat that can be conducted through the layer, so more heat must be transported by the slurry and greater temperatures are found in comparison to the higher thermal conductivity case.

Figure 3 shows a phase diagram of solutions to the steady state model comparing high and low thermal conductivity solutions. It shows that a wide range of solutions satisfy the geophysical constraints on the density jump and the CMB heat flux. Increasing the layer thickness increases the density jump across the layer at a fixed Q_s^i, and similar increases in density jump are observed when increasing Q_s^i for a fixed layer depth. There is a proportional increase in the CMB heat flux with layer thickness since a larger slurry volume releases more latent heat, and more secular cooling arises because the liquidus gradient is steeper than the adiabat. Very high estimates of the CMB heat flux are attained with $Q_s^i = 2$ TW for thicker layers with a high thermal conductivity.

Lower thermal conductivity models with smaller layer thicknesses can comfortably provide acceptable solutions with lower rates of inner core secular cooling. Less heat is conducted down the adiabat, and therefore more heat must be transported by the slurry compared to high thermal conductivity models. The temperature drop and hence the density jump increases across the layer in turn. Conversely, a higher thermal conductivity decreases the density jump across the layer significantly, since more heat is conducted along the adiabat and reduces the temperature drop across the slurry. A larger density jump requires a greater layer thickness and/or stronger heating from inner core secular cooling to compensate.

4 DISCUSSION

We have developed a simplified model of a slurry system to explain the dynamics of a seismically distinct layer at the base of the Earth's outer core. We propose that the F-layer can be explained by a slurry layer where stable stratification arises from particles of iron freezing out of the liquid alloy. As the iron particles fall under the influence of gravity, residual light element migrates towards the CSB into the rest of the outer core to help power the geodynamo. A steady state slurry zone that is chemically stable and on the liquidus temperature everywhere is consistent with the seismically inferred density jumps for a range of layer thicknesses and inner core secular cooling. Sensible values of the total CMB heat flux are achieved, using both high and low k. Greater layer thickness, secular cooling at the ICB and lower thermal conductivity tend to favour a larger density jump.

Several assumptions are made in order to produce a steady state slurry model, and these are appraised in the following discussion. These assumptions are

(i) fast-melting
(ii) constant solid
(iii) binary mixture
(iv) ideal solution theory
(v) fixed layer thickness
(vi) static slurry.

(i) The fast-melting limit considerably simplifies the thermodynamics and constrains the system to remain in phase equilibrium, hence the temperature follows the liquidus in the slurry. We expect that the timescale of melting and freezing is much shorter than the longer timescales (billions of years) of interest in the slurry. Without this limit departures from phase equilibrium must be incorporated into the constitutive relations using a macroscopic measure of the microscopic crystal growth process (Loper 1992). Nucleation may be a factor that can complicate the slurry model, in which fast-melting covers the need for supercooling and the provision of nucleation sites to overcome the energy barrier required to crystallize solid iron particles. Classical nucleation theory suggests that critical supercooling rates are as high as 1000 K for homogeneous nucleation (Huguet *et al.* 2018), which is so large that the inner core never freezes out. A less extreme position is that the degree of supercooling sufficient for nucleation is attained only at the ICB itself and a slurry never forms. Though possible it would be difficult to explain the F-layer, and it's not yet clear that a consistent thermal and compositional structure could be found in this case. Alfè *et al.* (2011) find no evidence of a barrier to melting/freezing using molecular dynamics simulations, and find that the mean waiting time to nucleate iron for a particular supercooling rate decreases as the system size increases. The degree of supercooling required to nucleate solid iron at core conditions during the onset of inner core freezing is poorly constrained, therefore the extent to which nucleation theory applies to the slurry model is limited in this period of the Earth's history. An initial slurry would be supercooled and the model equations presented in this paper will not apply. However once nucleation has occurred there will always be nucleation sites on which snow can grow, so supercooling becomes less of an issue. We believe, as did Roberts & Loper (1987), that once nucleation sites have been created the slurry will evolve to a mature slurry state in which fast-melting is a reasonable approximation to make.

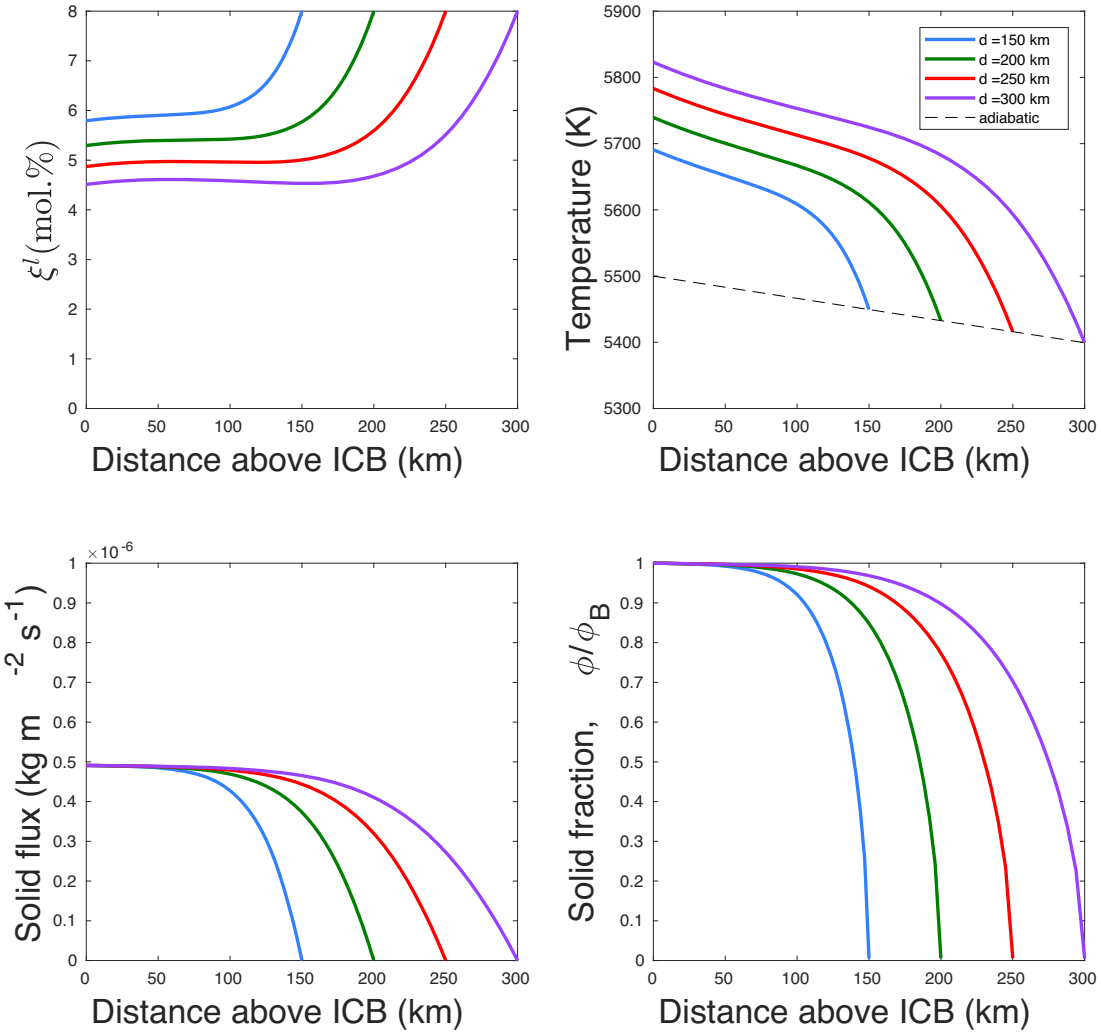

Figure 2 (Clockwise from top left) Profiles of ξ^l, temperature, solid fraction normalized by its value at the base of the layer, ϕ_B, and the solid flux. Layer thickness is indicated by the legend (colour online). Secular cooling of the inner core is fixed at $Q_s^i = 0.8\,\mathrm{TW}$ and the thermal conductivity is equal to $50\,\mathrm{W\,m^{-1}\,K^{-1}}$, with an inner core age of $\tau_i = 1\,\mathrm{Ga}$.

(ii) Core material is modelled as a simple binary mixture composed of iron and oxygen due to the constant solid assumption. The solid inner core is lighter than if it were made of pure iron (Jephcoat & Olson 1987) so partitioning other species of light element, such as silicon and sulphur, into the solid phase demands modelling of the composition history within each solid grain. This was not attempted in this study as modelling such a complex history significantly complicates the mathematical problem (Roberts & Loper 1987). However we expect the main dynamic effect is caused by the partitioning of oxygen when core material freezes, as this creates the compositional density contrast between solid and liquid for light element to rise out of the layer. We think that these approximations are sensible compromises given present knowledge of the core.

(iii) Ideal solution theory is used to estimate parameters that are difficult to measure experimentally at the relevant core pressures and temperatures, such as changes in density and the chemical potential. Ideal solutions exclude the possibility of chemical reactions between iron and light element. Whilst ideal solution theory is accurate for predicting densities, some studies suggest that it does not predict the chemical potential or its derivatives well at core conditions (Gubbins *et al.* 2004). Departures from ideal solution theory may steepen the liquidus curve and its intersection with the adiabat that controls the inner core growth rate, which may alter our results. Currently ideal solution theory is sufficient, though we expect parameter estimates to improve with future experiments.

(iv) Fixing the layer thickness at all times in a steady state model means that the entire slurry layer advances with the growing inner core at a constant speed. A turbulent mixing sublayer at the top with enhanced diffusion is introduced as a consequence, to enable a smooth transition at the CSB from a non-zero solid flux within the slurry to zero solid flux outside of the slurry. This allows the passage of light element from a high to low pressure environment, which balances the fresh light element brought into the top of the layer in the moving frame. Obtained solutions are not unique, and future studies could consider a CSB that moves at a speed separate to the ICB. Relaxing the steady state assumption allows the layer to grow or shrink over time, and eliminates the need for introducing a free parameter through the mixing layer. Considering the circumstances leading to layer growth may provide insight into the origins of the F-layer. Conditions surrounding a shrinking layer could indicate the timescale in which the layer may be diminishing, which could be longer than the timescales we can presently observe.

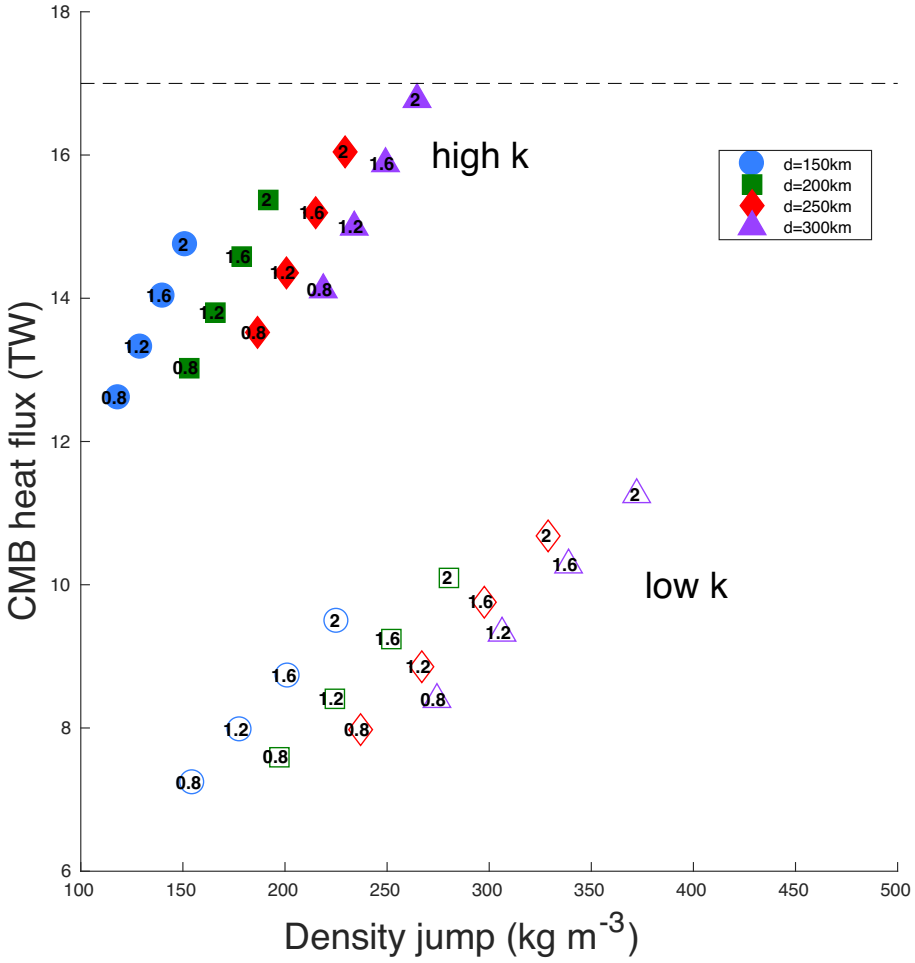

Figure 3 A phase diagram of steady state solutions of the slurry. Layer thicknesses are indicated by the symbols in the legend. The imposed inner core secular cooling (in TW) is given by the numbers enclosed. High conductivity solutions are grouped by filled in symbols, whereas low conductivity solutions are grouped by unfilled symbols. Along the x-axis is the calculated density jump and along the y-axis is the CMB heat flux. The maximum density jump inferred from seismology is 720 kg m^{-3} and the maximum plausible CMB heat flux is marked by the dashed line at 17 TW.

(v) The slurry is assumed to be static, however coupling the momentum equation (23i) to the system allows the convecting state to be investigated. Exploring its linear stability may map out the different regimes of slurry convection. Possible scenarios include a phase instability that can arise when lateral variations of solid phase induces overturning (Loper & Roberts 1987), or inner core convection from below could be connected to the model (Alboussière *et al.* 2010; Deguen *et al.* 2013). Nevertheless, maintaining a net stable stratification will remain a key requirement in such a convecting state in order to match the seismic observations.

Estimating mean solid particle size in models of particle mobility is important in characterizing the freezing process. It is unlikely that direct measurements of this property will be made in the Earth's core, however the advantage of our model is that we only need to resolve the solid flux. The model of mobility is used solely to relate the solid flux, $\mathbf{j}$, to the solid fraction, ϕ. Further work investigating the mobility may shed light on the range of admissible particle sizes encountered in the core. Estimates of particle sizes in alternative physical situations may benefit this problem—for example growth and coagulation of raindrops used in meteorology (Loper & Roberts 1977), and iron snow models in Ganymede (Ruckrieman *et al.* 2015).

If the model conditions (i)–(vi) are met, then a present-day slurry is likely to exist that can explain current geophysical observations. If $\mathrm{d}T_a/\mathrm{d}p < \mathrm{d}T_l/\mathrm{d}p < \mathrm{d}T_c/\mathrm{d}p$, where $\mathrm{d}T_l/\mathrm{d}p$ is the liquidus gradient and $\mathrm{d}T_c/\mathrm{d}p$ is the conduction gradient, then a slurry is inevitable (Loper & Roberts 1977). Estimates used in our current model for the thermal conductivity and ICB heat flux satisfy the above inequality. If $\mathrm{d}T_c/\mathrm{d}p < \mathrm{d}T_l/\mathrm{d}p$ then freezing may occur directly onto the core and a small conductive sublayer is possible. This case requires a very low heat flux near the ICB.

Under the fast-melting limit our slurry model idealizes that the inner core grows exclusively by solid particles settling at the ICB under Stokes flow. Alternatively it has been proposed that the inner core may grow through a mushy layer, where constitutional supercooling ahead of the ICB promotes dendritic crystal growth of solid iron at the interface (Fearn *et al.* 1981). The mushy solid matrix is permeated by interdendritic liquid channels, known as 'chimneys' that are enriched by residual light element (Mullins *et al.* 1964). The solid fraction of a mush is significantly greater than a slurry, as standard slurry theory considers $\phi \ll 1$. Deguen *et al.* (2007) conduct a linear stability analysis to find that the interdendritic spacing is at least several metres wide at the ICB in its current state, with an approximate layer thickness of 300 km extending below the ICB into the inner core. The top of the mush is coincident with the ICB

to be consistent with the sharpness of the seismic velocity jump at the ICB (Fearn *et al.* 1981), and the mush is thought to be strongly influenced by convection. Huguet *et al.* (2016) use experimental methods to suggest that mush convection is the dominant regime in the inner core, leaving a matrix with a solid fraction close to unity without the effect of compaction (a collapsing mush). If the inner core grows dendritically then a slurry layer cannot overlay a mush, since dendrites would grow to the point where the liquidus and adiabat intersect at the top of the F-layer which would have been seismically visible.

The steady-state slurry model presented here provides a good dynamic description of the present-day F-layer that agrees with current geophysical constraints. Further work testing our assumptions on how an evolving slurry layer couples to the thermal history of the Earth can answer the questions surrounding the origins of a slurry F-layer. Initial conditions surrounding F-layer formation may be probed, such as supercooling and the nucleation of the first stable iron crystal. Prior to inner core formation the adiabat may have initially crossed the liquidus to create a slurry at the centre of the Earth, or at an interior point away from the centre. If the latter is true, then the liquid core may entrain the slurry once it had formed from below the interior point by convection. Further work may also concern coupling the F-layer to the inner core and rest of the outer core, which may reveal potential feedback mechanisms.

ACKNOWLEDGEMENTS

JW is supported by the Engineering and Physical Sciences Research Council (EPSRC) Centre for Doctoral Training in Fluid Dynamics (EP/L01615X/1). CJD is supported by a Natural Environment Research Council (NERC) Independent Research Fellowship (NE/L011328/1). We thank Michael Bergman and an anonymous reviewer for their helpful comments on improving the paper.

REFERENCES

Adam, J.M.-C & Romanowicz, B., 2015. Global scale observations of scattered energy near the inner-core boundary: Seismic constraints on the base of the outer-core, *Phys. Earth planet. Inter.,* **245,** 103–116.

Alboussière, T., Deguen, R. & Melzani, M., 2010. Melting–induced stratification above the Earth's inner core due to convective translation, *Nature* **466,** 744–749.

Alfè, D., Cazorla, C. & Gillan, M.J., 2011. The kinetics of homogeneous melting beyond the limit of superheating, *J. Chem. Phys.,* **135,** 024102.

Alfè, D., Gillan, M.J. & Price, G.D., 2002a. Composition and temperature of the Earth's core constrained by combining *ab initio* calculations and seismic data, *Earth planet. Sci. Lett.,* **195,** 91–98.

Alfè, D., Gillan, M.J. & Price, G.D., 2002b. Composition and temperature of the Earth's core constrained by combining *ab initio* calculations and seismic data, *Earth planet. Sci. Lett.,* **195,** 91–98.

Anufriev, A.P., Jones, C.A. & Soward, A.M., 2005. The Boussinesq and anelastic liquid approximations for convection in the Earth's core, *Phys. Earth planet. Inter.,* **152,** 163–190.

Badro, J., Brodholt, J.P., Piet, H., Siebert, J. & Ryerson, F.J., 2015. Core formation and core composition from coupled geochemical and geophysical constraints, *Proc. Natl. Acad. Sci. U.S.A.,* **112,** 12 310–12 314.

Davies, C. & Pommier, A., 2018. Iron snow in the Martian core?, *Earth planet. Sci. Lett.,* **481,** 189–200.

Davies, C., Pozzo, M., Gubbins, D. & Alfè, D., 2015. Constraints from material properties on the dynamics and evolution of Earth's core, *Nature Geoscience,* **8,** 678–685.

Deguen, R., Alboussière, T. & Brito, D., 2007. On the existence and structure of a mush at the inner core boundary of the Earth, *Phys. Earth planet. Inter.,* **164,** 36–49.

Deguen, R., Alboussière, T. & Cardin, P., 2013. Thermal convection in Earth's inner core with phase change at its boundary, *Geophys. J. Int.,* **194,** 1310–1334.

Deuss, A., 2014. Heterogeneity and anisotropy of Earth's inner core, *Annu. Rev. Earth planet. Sci.,* **42,** 103–126.

Dziewonski, A.M. & Anderson, D.L., 1981. Preliminary reference Earth model, *Phys. Earth planet. Inter.,* **25,** 297–356.

Fearn, D.R., Loper, D.E. & Roberts, P.H., 1981. Structure of the Earth's inner core, *Nature,* **292,** 232–233.

Gomi, H., Ohta, K., Hirose, K., Labrosse, S., Caracas, R., Verstraete, M.J. & Hernlund, J.W., 2003. The high conductivity of iron and thermal evolution of the Earth's core, *Phys. Earth planet. Inter.,* **224,** 88–103.

Gubbins, D., Alfè, D. & Davies, C.J., 2013. Compositional instability of Earth's solid inner core, *Geophys. Res. Lett.,* **40,** 1084–1088.

Gubbins, D., Alfè, D., Masters, G., Price, G.D. & Gillan, M.J., 2003. Can the Earth's dynamo run on heat alone? , *Geophys. J. Int.,* **155**(2), 609–622.

Gubbins, D., Alfè, D., Masters, T.G. & Price, D., 2004. Gross thermodynamics of two-component core convection, *Geophys. J. Int.,* **157,** 1407–1414.

Gubbins, D., Masters, T.G. & Nimmo, F., 2008. A thermochemical boundary layer at the base of Earth's outer core and independent estimate of core heat flux, *Geophys. J. Int.,* **174,** 1007–1018.

Huguet, L., Alboussière, T., Bergman, M.I., Deguen, R., Labrosse, S. & Lesœur, G., 2016. Structure of a mushy layer under hypergravity with implications for Earth's inner core, *Geophys. J. Int.,* **204,** 1729–1755.

Huguet, L., Van Orman, J.A., Hauck, S.A., II & Willard, M.A., 2018. Earth's inner core nucleation paradox, *Earth planet. Sci. Lett.,* **487,** 9–20.

Jephcoat, A. & Olson, P., 1987. Is the inner core of the Earth pure iron?, *Nature,* **325**(6102), 332–335.

Kennett, B.L.N., Engdahl, E.R. & Buland, R., 1995. Constraints on seismic velocities in the Earth from traveltimes, *Geophys. J. Int.,* **122,** 108–124.

Konôpková, Z., McWilliams, R. S., Gómez-Pérez, N. & Goncharov, A.F., 2016. Direct measurement of thermal conductivity in solid iron at planetary core conditions, *Nature,* **534**(7605), 99–101.

Koper, K. & Dombrovskaya, M., 2005. Seismic properties of the inner core boundary from PKiKP/P amplitude ratios, *Earth planet. Sci. Lett.,* **237,** 680–694.

Koper, K. & Pyle, M., 2004. Observations of PKiKP/PcP amplitude ratios and implications for Earth structure at the boundaries of the liquid core, *J. geophys. Res.,* **109**(B3).

Labrosse, S., 2014. Thermal and compositional stratification of the inner core, *C.R. Geosci.,* **346,** 119–123.

Labrosse, S., Poirier, J.P. & Le Mouël, J.-L., 2001. The age of the inner core, *Earth planet. Sci. Lett.,* **190,** 111–123.

Landau, L.D. & Lifshitz, E.M., 1959. Course of Theoretical Physics, in *Vol. 6: Fluid Mechanics,* Pergammon, London.

Lay, T., Hernlund, J. & Buffett, B.A., 2008. Core-mantle boundary heat flow, *Nat. Geosci.,* **1** 25–32.

Loper, D.E., , & Roberts, P.H., 1987. A Boussinesq model of a slurry, in *Structure and Dynamics of Partially Solidified Systems,* Martinus Nijhoff Publishers, Loper, D.E., pp. 293–323.

Loper, D.E., 1992. A nonequilibrium theory of a slurry, *Continuum Mech. Thermodyn.,* **4**(3) 213–245.

Loper, D.E. & Roberts, P.H., 1977. On the motion of an iron-alloy core containing a slurry. 1: general theory, *Geophys. Astrophys. Fluid Dyn.,* **9,** 289–321.

Loper, D.E. & Roberts, P.H., 1980. On the motion of an iron-alloy core containing a slurry. 2: a simple model, *Geophys. Astrophys. Fluid Dyn.,* **16,** 83–127.

Lythgoe, K.H., Rudge, J.F., Neufeld, J.A. & Deuss, A., 2015. The feasibility of thermal and compositional convection in Earth's inner core, *Geophys. J. Int.,* **201,** 764–782.

Masters, T.G. & Gubbins, D., 2003. On the resolution of density within the Earth, *Phys. Earth planet. Inter.,* **140,** 159–167.

Mullins, W.W. & Sekerka, R.F., 1964. Stability of a planar interface during solidification of a dilute binary alloy, *J. appl. Phys.,* **35,** 444–451.

Nimmo, F., 2015. Energetics of the core, in *Treatise on Geophysics,* Vol. **8,** Elsevier, Schubert, G., pp. 27–55 (2nd edn).

Ohtaki, T. & Kaneshima, S., 2015. Independent estimate of velocity structure of Earth's lowermost outer core beneath the northeast Pacific from PKiKP–PKPbc differential traveltime and dispersion in PKPbc, *J. geophys. Res.,* **120,** 7572–7586.

Pourovskii, L.V., Mravlje, J., Georges, A., Simak, S.I. & Abrikosov, I.A., 2017. Electron-electron scattering and thermal conductivity of ϵ-iron at Earth's core condition, *New J. Phys.,* **19,** 073022.

Pozzo, M., Davies, C., Gubbins , D. & Alfè, D., 2013. Transport properties for liquid silicon-oxygen-iron mixtures at Earth's core conditions, *Phys. Rev. B,* **87,** 014110.

Pozzo, M., Davies, C., Gubbins, D. & Alfé, D., 2014. Thermal and electrical conductivity of iron at Earth's core conditions, *Nature,* **485,** 355–358.

Roberts, P.H. & Loper, D.E., 1987. Dynamical processes in slurries, in *Structure and Dynamics of Partially Solidfied Systems,* Martinus Nijhoff Publishers, Loper, D.E., pp. 229–290.

Rückrieman, T., Breuer, F. & Spohn, T., 2015. The Fe snow regime in Ganymede's core: a deep-seated dynamo below a stable snow zone, *J. geophys. Res.,* **120,** 1095–1118.

Solomatov, V.S., 2015. Magma oceans and primordial mantle differentiation, in *Treatise on Geophysics,* Vol. **9,** Elsevier, Schubert, G., pp. 81–104, 2nd edn.

Song, X.D. & Helmberger, D.V., 1992. Velocity structure near the inner core boundary from wave-form modelling, *J. geophys. Res.,* **97,** 6573–6586.

Souriau, A. & Poupinet, G., 1991. The velocity profile at the base of the liquid core from PKP(BC+Cdiff) data – an argument in favour of radial inhomogeneity, *Geophys. Res. Lett.,* **18,** 2023–2026.

Tkalčić, H., Kennett, B.L.N. & Cormier, V.F., 2009. On the inner-outer core density contrast from PKiKP/PcP amplitude ratios and uncertainties caused by seismic noise, *Geophys. J. Int.,* **179,** 425–443.

Zou, Z., Koper, K.D. & Cormier, V.F., 2008. The structure at the base of the outer core inferred from seismic waves diffracted around the inner core, *J. geophys. Res.,* **113,** B5.

APPENDIX: THERMODYNAMIC RELATIONS

Consider the Gibbs free energy, Φ, where the pressure, p, temperature, T, concentration of light material, ξ and solid fraction ϕ are chosen to be the independent thermodynamic variables of the slurry system. The differential of the Gibbs free energy under the constant solid assumption ($\xi^s = 0$) is

$$\begin{aligned} \mathrm{d}\Phi &= \left(\frac{\partial \Phi}{\partial p}\right)_{T,\xi,\phi} \mathrm{d}p + \left(\frac{\partial \Phi}{\partial T}\right)_{p,\xi,\phi} \mathrm{d}T \\ &\quad + \left(\frac{\partial \Phi}{\partial \xi}\right)_{p,T,\phi} \mathrm{d}\xi + \left(\frac{\partial \Phi}{\partial \phi}\right)_{p,T,\xi} \mathrm{d}\phi \\ &= V\mathrm{d}p - s\mathrm{d}T + \mu \mathrm{d}\xi + (\mu_\phi + \xi^l \mu)\mathrm{d}\phi \end{aligned} \tag{A1}$$

where V is the specific volume, s is the entropy, μ is the chemical potential of iron relative to light material in the liquid, and μ_ϕ is the chemical potential of the solid phase relative to the liquid phase.

The Gibbs free energy is a thermodynamic potential that yields the differentials of the specific volume, $\mathrm{d}V$, entropy, $\mathrm{d}s$, and chemical potential, $\mathrm{d}\mu$, required by the slurry theory. The differential of the specific volume gives the density variation, ρ', in (23j) and is given by

$$\begin{aligned} \mathrm{d}V &\equiv \mathrm{d}\rho^{-1} \\ &= \frac{\alpha}{\rho^l_{\mathrm{Fe}}}\mathrm{d}T + \frac{\alpha_\xi}{\rho^l_{\mathrm{Fe}}}\mathrm{d}\xi - \frac{\alpha_\phi}{\rho^l_{\mathrm{Fe}}}\mathrm{d}\phi \\ &= \frac{\alpha}{\rho^l_{Fe}}\mathrm{d}T + \frac{\alpha_\xi(1-\phi)}{\rho^l_{\mathrm{Fe}}}\mathrm{d}\xi^l - \left(\frac{\alpha_\phi}{\rho^l_{\mathrm{Fe}}} + \frac{\alpha_\xi \xi^l}{\rho_0}\right)\mathrm{d}\phi \end{aligned} \tag{A2}$$

where

$$\frac{\alpha}{\rho^l_{\mathrm{Fe}}} \equiv \left(\frac{\partial V}{\partial T}\right)_{p,\xi,\phi}, \qquad \frac{\alpha_\xi}{\rho^l_{\mathrm{Fe}}} \equiv \left(\frac{\partial V}{\partial \xi}\right)_{p,T,\phi}$$

and the phasal coefficient α_ϕ arises from the non-natural thermodynamic derivative, manipulated using (2) along with the definition of $\Delta V^{s,l}_{\mathrm{Fe}}$ (A12) to give

$$\begin{aligned} -\frac{\alpha_\phi}{\rho^l_{\mathrm{Fe}}} &\equiv \left(\frac{\partial V}{\partial \phi}\right)_{T,\xi} \\ &= \left(\frac{\partial V}{\partial \xi^l}\right)_{T,\phi}\left(\frac{\partial \xi^l}{\partial \phi}\right)_{\xi} + \left(\frac{\partial V}{\partial \phi}\right)_{T,\xi} \\ &= -\frac{\xi^l \alpha_\xi}{\rho^l_{\mathrm{Fe}}(1-\phi)} + \frac{\partial}{\partial \phi}\left(\frac{\partial \Phi}{\partial p}\right)_{T,\xi,\phi} \\ &= -\frac{\xi^l \alpha_\xi}{\rho^l_{Fe}(1-\phi)} + \frac{\partial}{\partial p}\left(\frac{\partial \Phi}{\partial \phi}\right)_{p,T,\xi} \\ &= -\frac{\xi^l \alpha_\xi}{\rho^l_{Fe}(1-\phi)} + \left(\frac{\partial}{\partial p}(\mu_\phi + \xi^l \mu)\right)_{T,\xi^l} \\ &= -\left(\frac{\xi^l \alpha_\xi}{\rho^l_{\mathrm{Fe}}(1-\phi)} + \Delta V^{s,l}_{\mathrm{Fe}}\right). \end{aligned} \tag{A3}$$

Note that density variations due to pressure, $\mathrm{d}p$, are assumed to be negligible in the Boussinesq approximation in (A2).

The entropy differential is used to complete the energy equation (23d), and is manipulated in a similar manner to give

$$\mathrm{d}s = -\frac{\alpha}{\rho^l_{\mathrm{Fe}}}\mathrm{d}p + \frac{c_p}{T}\mathrm{d}T + (1-\phi)\frac{\partial \mu}{\partial T}\mathrm{d}\xi^l - \left(\xi^l \frac{\partial \mu}{\partial T} + \frac{L}{T}\right)\mathrm{d}\phi \tag{A4}$$

where

$$-\frac{\alpha}{\rho^l_{\mathrm{Fe}}} \equiv \left(\frac{\partial s}{\partial p}\right)_{T,\xi^l,\phi}, \qquad \frac{c_p}{T} \equiv \left(\frac{\partial s}{\partial T}\right)_{p,\xi^l,\phi},$$
$$(1-\phi)\frac{\partial \mu}{\partial T} \equiv \left(\frac{\partial s}{\partial \xi^l}\right)_{p,T,\phi}, \qquad -\left(\xi^l \frac{\partial \mu}{\partial T} + \frac{L}{T}\right) \equiv \left(\frac{\partial s}{\partial \phi}\right)_{p,T,\xi^l}.$$

The chemical potential differential is used in the flux vectors $\mathbf{i}$, $\mathbf{j}$ and $\mathbf{k}$ in eqs (18), (19) and (21). This is given by

$$\mathrm{d}\mu = \Delta V^l_{\mathrm{Fe,O}}\mathrm{d}p + \left(\frac{\partial \mu}{\partial T}\right)_{p,\xi^l\phi}\mathrm{d}T + \left(\frac{\partial \mu}{\partial \xi^l}\right)_{p,T,\phi}\mathrm{d}\xi^l, \tag{A5}$$

where

$$\Delta V^l_{\mathrm{Fe,O}} \equiv \left(\frac{\partial \mu}{\partial p}\right)_{T,\xi^l,\phi}.$$

The Lever rule allows a significant simplification by assuming that the liquid and solid phases do not interact chemically. As a result, the Gibbs free energy is linear in ϕ and we can write

$$\Phi = \phi\Phi^s(p,T) + (1-\phi)\,\Phi^l(p,T,\xi^l), \tag{A6}$$

where Φ^s is the solid part of the Gibbs free energy and Φ^l is the liquid part of the Gibbs free energy. Its exact differential is

$$\mathrm{d}\Phi = \phi\mathrm{d}\Phi^s + (1-\phi)\mathrm{d}\Phi^l + \left(\Phi^s - \Phi^l\right)\mathrm{d}\phi. \tag{A7}$$

In terms of the independent thermodynamic variables p, T, ξ^l and ϕ, (A7) is equivalent to

$$d\Phi = \left(\phi\frac{\partial\Phi^s}{\partial p} + (1-\phi)\frac{\partial\Phi^l}{\partial p}\right)\mathrm{d}p + \left(\phi\frac{\partial\Phi^s}{\partial T} + (1-\phi)\frac{\partial\Phi^l}{\partial T}\right)\mathrm{d}T + \frac{\partial\Phi^l}{\partial\xi^l}\mathrm{d}\xi^l + \left(\Phi^s - \Phi^l + \xi^l\frac{\partial\Phi^l}{\partial\xi^l}\right)\mathrm{d}\phi. \tag{A8}$$

By comparing this with (A1), it can be seen that the specific volume, V, entropy, s, and chemical potential, μ, follow a similar lever rule with

$$V^s \equiv \left(\frac{\partial\Phi^S}{\partial p}\right)_T, \qquad V^l \equiv \left(\frac{\partial\Phi^L}{\partial p}\right)_{T,\xi^l},$$
$$-s^s \equiv \left(\frac{\partial\Phi^s}{\partial T}\right)_p, \qquad -s^l \equiv \left(\frac{\partial\Phi^l}{\partial T}\right)_{p,\xi^l},$$
$$\mu \equiv \left(\frac{\partial\Phi^l}{\partial\xi^l}\right)_{p,T}, \qquad \mu_\phi \equiv \Phi^s - \Phi^l.$$

At phase equilibrium, the Gibbs free energy is minimized and therefore $\mathrm{d}\Phi = 0$. By the fast-melting limit, a change in phase is assumed to be instantaneous, so at constant pressure, temperature and light material, a variation of the solid fraction ($\mathrm{d}\phi \neq 0$) requires that

$$\mu_\phi + \xi^l\mu = 0. \tag{A9}$$

By comparison with (A8), this condition is equivalent to

$$\Phi^s - \Phi^l + \xi^l\frac{\partial\Phi^l}{\partial\xi^l} = 0. \tag{A10}$$

The differential (A10) is also equal to zero at phase equilibrium, so

$$\left(V^s - V^l\right)\mathrm{d}p - \left(s^s - s^l\right)\mathrm{d}T + \xi^l\left(\Delta V^l_{\mathrm{Fe,O}}\mathrm{d}p + \frac{\partial\mu}{\partial T}\mathrm{d}T + \frac{\partial\mu}{\partial\xi^l}\mathrm{d}\xi^l\right) = 0 \tag{A11}$$

through the Lever rule and the definition of $\mathrm{d}\mu$ (A5). We define

$$-\Delta V^{s,l}_{\mathrm{Fe}} = -\Delta V^{s,l}_{\mathrm{Fe,O}} + \xi^l\Delta V^l_{\mathrm{Fe,O}} \tag{A12}$$

as the change in specific volume between the solid and liquid iron, $-\Delta V^{s,l}_{\mathrm{Fe,O}} = V^s - V^l$, is the change in specific volume between the solid and liquid phase and $\Delta V^l_{\mathrm{Fe,O}}$ is the change in specific volume between light element and liquid iron. Similarly,

$$\frac{L}{T} = -s^s + s^l + \xi^l\frac{\partial\mu}{\partial T} \tag{A13}$$

defines the latent heat. The phase equilibrium condition (A11) therefore yields the liquidus

$$\xi^l\frac{\partial\mu}{\partial\xi^l}\mathrm{d}\xi^l = \Delta V^{s,l}_{\mathrm{Fe}}\mathrm{d}p - \frac{L}{T}\mathrm{d}T. \tag{A14}$$

Table A1. Commonly used symbols and estimates of slurry properties. For ease of reference, the corresponding symbols used in Loper & Roberts (1977, 1980, 1987) is provided in brackets.

Symbol	Definition	Estimate	Units	Source
ξ	Light element concentration			
ξ^l	Light element concentration in the liquid phase			
ϕ	Solid fraction			
T	Temperature		K	
p	Pressure		Pa	
$\mathbf{u}$	Flow velocity		$\mathrm{m\,s^{-1}}$	
r_i	ICB radius	1.22×10^6	m	PREM (Dziewonski & Anderson 1981)
r_o	CMB radius	3.48×10^6	m	PREM
d	Layer depth	$1.5–3 \times 10^5$	m	Souriau & Poupinet (1991), etc.
$g\rho^l_{\mathrm{Fe}}$	Hydrostatic pressure gradient at $r = r_i$	5.51×10^4	$\mathrm{Pa\,m^{-1}}$	PREM
$\Delta\rho_{\mathrm{melting}}$	Density drop upon melting	0.24×10^3	$\mathrm{kg\,m^{-3}}$	Alfè *et al.* (2002b)
β	Isothermal compressibility	7.55×10^{-13}	$\mathrm{Pa^{-1}}$	Gubbins *et al.* (2008)
ρ_O	Specific density of light element	5.56×10^3	$\mathrm{kg\,m^{-3}}$	Gubbins *et al.* (2004)
ρ^l_{Fe}	Specific density of liquid iron, reference density	12.52×10^3	$\mathrm{kg\,m^{-3}}$	Gubbins *et al.* (2004)
ρ^s_{Fe} (ρ^s)	Specific density of solid	12.76×10^3	$\mathrm{kg\,m^{-3}}$	Gubbins *et al.* (2004)
$\Delta V^l_{\mathrm{Fe,O}}$ ($\bar{\delta}$)	Change in specific volume between light element and liquid iron	10.00×10^{-5}	$\mathrm{kg^{-1}\,m^3}$	
$\Delta V^{s,l}_{\mathrm{Fe,O}}$ (ΔV)	Change in specific volume between liquid and solid phase	4.03×10^{-6}	$\mathrm{kg^{-1}\,m^3}$	
$\Delta V^{s,l}_{\mathrm{Fe}}$ (δ)	Change in specific volume between liquid iron and solid iron	1.50×10^{-6}	$\mathrm{kg^{-1}\,m^3}$	
c_p (C_p)	Specific heat capacity	715	$\mathrm{J\,kg^{-1}\,K^{-1}}$	Gubbins *et al.* (2003)
α	Thermal expansion coefficient	1×10^{-5}	$\mathrm{K^{-1}}$	Davies *et al.* (2015)
α_ξ ($\bar{\alpha}$)	Compositional expansion coefficient	1.1		Nimmo (2015)
α_ϕ	Phasal expansion coefficient	0.02		
μ (μ^l)	Chemical potential of light element relative to iron		$\mathrm{J\,kg^{-1}}$	
$\partial\mu/\partial\xi^l$ ($\bar{\mu}$)	Thermodynamic derivative of chemical potential w.r.t. ξ^l	$\mathrm{J\,kg^{-1}}$	Gubbins *et al.* (2004)	
μ_0	Constant used in the logarithmic form of the chemical potential			
μ_ϕ (ψ)	Chemical potential of solid relative to the liquid		$\mathrm{J\,kg^{-1}}$	
k	Thermal conductivity	50–107	$\mathrm{W\,m^{-1}\,K^{-1}}$	Davies *et al.* (2015), Konôpkova *et al.* (2016)
L	Latent heat of fusion	0.75×10^6	$\mathrm{J\,kg^{-1}}$	Davies *et al.* (2015)
D'	ξ^l self–diffusion coefficient (dependent on ϕ)		$\mathrm{m^2\,s^{-1}}$	
$\bar{D}$	Modified self–diffusion ξ^l coefficient (independent of ϕ)		$\mathrm{m^2\,s^{-1}}$	
D_0	ξ^l self–diffusion coefficient	1×10^{-8}	$\mathrm{m^2\,s^{-1}}$	Pozzo *et al.* (2013)
F	Turbulent mixing coefficient			
ξ_T	Light element fraction at the top of the slurry layer (assumed to be 8 mol. per cent O)	0.0252		Alfè *et al.* (2002b)
v	Speed of ICB advance	1.2–2.4	$\mathrm{mm\,yr^{-1}}$	
τ_i	Inner core age	0.5–1	Ga	Gomi *et al.* (2013)
T_i	Temperature at ICB	5500	K	Nimmo (2015)
T_a	Adiabatic temperature		K	
Q^i_s	ICB heat flux (inner core secular cooling excluding the latent heat flux)	0.8–2	TW	
Q^c	CMB heat flux	12 ± 5	TW	Lay *et al.* (2008)
Q_s	Secular cooling		TW	
Q_l	Latent heat flux		TW	
Q_g	Gravitational power		TW	
$\mathbf{n}$	Unit normal to the boundary of the ICB, pointing into the slurry			
$\mathbf{i}$	Light element flux vector		$\mathrm{kg\,m^{-2}\,s^{-1}}$	
$\mathbf{j}$	Solid mass flux vector		$\mathrm{kg\,m^{-2}\,s^{-1}}$	
$\mathbf{k}$	Entropy flux vector		J	
$b(\phi)$	Sedimentation coefficient		$\mathrm{kg\,m^{-3}\,s}$	
m^s	Creation rate of solid particles		$\mathrm{kg\,m^{-3}\,s^{-1}}$	
M^l_{O}	Mass of oxygen		kg	
M^l_{Fe}	Mass of liquid iron		kg	
M^s_{Fe}	Mass of solid iron		kg	
ρ'	Density variation		$\mathrm{kg\,m^{-3}}$	
Φ	Gibbs free energy		J	
V	Specific volume		$\mathrm{m^3\,kg^{-1}}$	
s	Entropy		$\mathrm{J\,K^{-1}}$	
R	Gas constant	8.31	$\mathrm{J\,K^{-1}\,mol^{-1}}$	